J. Wind Eng. Ind. Aerodyn. 122 (2013) 2–9

Contents lists available at ScienceDirect

Journal of Wind Engineering and Industrial Aerodynamics

journal homepage: www.elsevier.com/locate/jweia

Vorticity generation and wake transition for a translating circular cylinder: Wall proximity and rotation effects

K. Hourigan [a,b,*], A. Rao [a], M. Brøns [c], T. Leweke [d], M.C. Thompson [a]

[a] Fluids Laboratory for Aeronautical and Industrial Research (FLAIR), Department of Mechanical and Aerospace Engineering, Monash University, Clayton, Victoria 3800, Australia
[b] Division of Biological Engineering, Monash University, Clayton 3800, Australia
[c] Department of Mathematics, Technical University of Denmark, Lyngby DK-2800, Denmark
[d] IRPHE UMR 7342, CNRS, Aix-Marseille Université, 13384 Marseille, France

ARTICLE INFO

Available online 17 July 2013

Keywords:
Vorticity
Bluff bodies
Wakes
Stability

ABSTRACT

The wake transitions of generic bluff bodies, such as a circular cylinder, near a wall are important because they provide understanding of different transition paths towards turbulence, and give some insight into the effect of surface modifications on the flow past larger downstream structures. In this article, the fundamentals of vorticity generation and transport for the two-dimensional flow of incompressible Newtonian fluids are initially reviewed. Vorticity is generated only at boundaries by tangential pressure gradients or relative acceleration. After generation, it can cross-annihilate with opposite-signed vorticity, and can be stored at a free surface, thus conserving the total vorticity, or circulation. Vorticity generation, diffusion and storage are demonstrated for a cylinder translating and rotating near a wall. The wake characteristics and the wake transitions are shown to change dramatically under the influence of cylinder rotation and wall proximity. At gaps between the cylinder and the wall of less than approximately 0.25 cylinder diameter, the wake becomes three dimensional prior to becoming unsteady, while for larger gaps the initial transition is to an unsteady two-dimensional wake. At a gap of 0.3 cylinder diameter, we observe a sharp increase in the critical Reynolds number at which three-dimensionality sets in. As the gap is further increased, the critical Reynolds number initially decreases before increasing to that for an isolated cylinder. The effect of cylinder rotation on these transitions is also quantified, with forward (prograde) rotation enhancing three-dimensional instability and reverse (retrograde) rotation stabilising the wake. High retrograde rotation leads to suppression of three-dimensional flow until beyond the highest Reynolds number investigated ($Re=750$).

1. Introduction

Fundamental to understanding flows around, and forces on, stalled airfoils and bluff bodies in aeronautics and wind engineering are the wake flow structures and the transitions between different wake modes, which substantially control wake development. The circular cylinder is a generic bluff body that has been used extensively to gain insight into the effect of these transitions on the wake. The classic theoretical model is an infinite cylinder, in practice experimentally modelled by high aspect ratio cylinders in wind or water tunnels (and, of course, cylindrical geometry is clearly the basis of the design of tall buildings for very high Reynolds number flows). The current paper focusses on much lower Reynolds number flows, with direct relevance to understanding wall-particle interactions that commonly occur in industrial processes such as sedimentation and mixing tanks, heat exchangers, etc). The Reynolds number for these latter applications is $Re=UD/\nu=O(10^2–10^3)$, where U is the velocity, D is the characteristic length and ν is the kinematic viscosity of the fluid. Experimental results at higher Reynolds numbers often show that the initial three-dimensional instability modes for these simplified geometries are still present and strongly influence the fully turbulent flow. For instance, *mode B*, which appears in a cylinder wake at $Re\approx230$ persists and is observable at much higher Reynolds number when the flow is fully turbulent (e.g., Wu et al., 1996), whilst the Strouhal number of the wake remains approximately constant over the range $200\leq Re\leq10^5$ (e.g., Batchelor, 1967). Thus, as well as their direct relevance to specific industrial applications, the results from such studies may eventually assist with interpreting higher Reynolds number flows in vehicular aerodynamics, flow past low rise buildings, surface

* Corresponding author at: Fluids Laboratory for Aeronautical and Industrial Research (FLAIR), Department of Mechanical and Aerospace Engineering, Monash University, Clayton, Victoria 3800, Australia. Tel.: +61 399 0596 24; fax: +61 399 0597 24.
E-mail address: kerry.hourigan@monash.edu (K. Hourigan).

0167-6105/$ - see front matter
http://dx.doi.org/10.1016/j.jweia.2013.06.009

roughness effects of mounted structures over roofs of buildings, etc.

Vorticity is one of the most important physical quantities in fluid mechanics used to characterise a flow. Boundary layers, wakes and turbulence in bluff body flows owe their presence to, and are essentially defined by, vorticity and vortices, whose motions are associated with fluctuating forces in a flow, including those leading to VIV (Vortex induced vibration). To understand wake structures and transitions, and how they can be controlled, it is important to determine and understand the mechanism of vorticity generation and its subsequent evolution. In this study, we focus on the canonical geometry of a circular cylinder to gain an understanding of the variety of wake structures and transitions that arise as the influence of both wall proximity and cylinder rotation are increased.

The flow past a circular cylinder in freestream has been widely investigated through both experimental (Williamson, 1988, 1996; Roshko, 1954) and numerical techniques (Karniadakis and Trintafyllou, 1992; Thompson et al., 1996; Barkley and Henderson, 1996). At low Reynolds numbers, steady flow is observed with the formation of two recirculation regions in the near wake until $Re \approx 47$. Beyond this Reynolds number, unsteady flow is observed. Vortices are alternately shed into the wake from the cylinder leading to the classical Bénard–von Kármán wake. Around $Re = 190$, the flow becomes three-dimensional with a spanwise wavelength of approximately four cylinder diameters; this instability is commonly referred to as the *mode A* instability (Barkley and Henderson, 1996; Williamson, 1988, 1996; Thompson et al., 1996). At slightly higher Reynolds number, $Re \approx 230$–240, a short wavelength instability develops with a spanwise wavelength of approximately one diameter on the already three-dimensional wake, and this has been termed *mode B*. The equivalent two transitions to three-dimensional flow have been observed in other bluff bodies wakes such as for square and elliptical cylinders, which undergo these transitions at slightly lower Reynolds numbers.

For a rotating circular cylinder in freestream, the onset of vortex shedding depends on the combination of the Reynolds number and the rotation rate, α, where $\alpha = \omega D/2U$, the ratio of the surface tangential velocity to the freestream flow speed. The critical Reynolds number at which periodic flow is observed is delayed to higher Reynolds number as the rotation rate is increased (Kang et al., 1999). For $\alpha \gtrsim 2$, vortex shedding was suppressed even at high Reynolds numbers (Akoury et al., 2008; Pralits et al., 2010) and the flow remains steady. However, at still higher rotation rates, a secondary shedding regime was observed for $\alpha \gtrsim 4.35$ (Mittal and Kumar, 2003; Stojković et al., 2003; Akoury et al., 2008; Kumar et al., 2011). In this shedding regime, single-sided vortex shedding occurs by release of positive vorticity into the wake at a low shedding frequency. For $\alpha \gtrsim 5.5$, the flow remains steady. For a rotating cylinder, the onset of three-dimensionality has been well documented in a recent investigation by Rao et al. (2013) for $\alpha \leq 2.5$. While mode A and mode B instabilities are delayed to higher Reynolds numbers at low rotation rates, a subharmonic mode becomes unstable for $\alpha \approx 1.5$. Two other three-dimensional modes, whose spatio-temporal characteristics are similar to the mode A instability, occur on the unsteady base flow, and two other modes are observed on the steady base flow for $\alpha \gtrsim 2$.

Although the flow structures and the forces on a body in isolation have been well documented, fewer investigations have been performed for bodies near a plane boundary. One of the earliest investigations for bodies moving near a wall was made by Taneda (1965), who observed the flow structures for a circular cylinder translating along a wall at $Re = 170$. For the cylinder very close to a wall ($G/D = 0.1$), a single-sided vortex street was observed. Here, G/D is the non-dimensionalised gap height, where the distance between the cylinder and the wall is G and the cylinder diameter is D. The vortices were unstable and diffused as they convected downstream.

Experimental investigations were performed by Bearman and Zdravkovich (1978) for a cylinder near a fixed wall at $Re = 4.5 \times 10^4$ for $0 \leq G/D \leq 3.5$. The cylinder was located approximately $36D$ from the start of a turbulent boundary layer, which developed along the wall. They observed the suppression of regular vortex shedding for $G/D < 0.3$, with the Strouhal number remaining constant until this gap height was approached. Bailey et al. (2002) performed experimental investigations for a square cylinder near a stationary wall at $Re = 18{,}900$ and observed that the flow becomes increasingly two-dimensional in the range $0.53 \leq G/D \leq 0.7$.

Using a finite-difference method, Lei et al. (2000) performed numerical simulations for a circular cylinder for gap heights between $0.1 \leq G/D \leq 3$ and Reynolds numbers between $80 \leq Re \leq 1000$. The frame of reference was such that the flow moved past the fixed lower wall and the cylinder, leading to the development of a boundary layer ($16D$ upstream of the cylinder). They observed that the gap height at which vortex shedding was suppressed decreased as the Reynolds number was increased up to $Re = 600$. Beyond this value, the critical gap height remained constant. At higher Reynolds numbers, Price et al. (2002) observed periodicity in the upper shear layer for all gap heights $G/D > 0.125$. While the pairing of shear layers from either side of the cylinder was observed for $0.25 \leq G/D \leq 0.375$, vortex shedding was observed at higher gap heights of $G/D > 0.5$.

Mahir (2009) investigated the onset of three-dimensional flow for a square cylinder near a fixed wall for $Re \leq 250$ as the gap height was increased from $0.1 \leq G/D \leq 4$. At $Re = 185$, mode A type vortex structures with spanwise spacing of $\approx 3D$ were observed for gap heights greater than $G/D = 1.2$, while at $G/D = 0.8$, mode B type vortex structures of $1D$ spanwise wavelength were observed. Below $G/D = 0.5$, neither mode A nor B type vortex structures were observed. At $Re = 250$, mode B type vortex structures were observed at larger gap heights, while at lower gap heights, the vortex structure was distorted in the vicinity of the cylinder.

Cheng and Luo (2007) investigated the flow structures and forces on a rotating circular cylinder near a wall at $Re = 200$. As the cylinder was moved away from the wall, they observed the suppression of vortex shedding ($G/D \approx 0.5$), followed by a region of aperiodic vortex shedding and finally a region of alternate Bénard–von Kármán shedding ($G/D \approx 1.5$). They further quantified the lift and drag coefficients experienced by the cylinder.

Experimental investigations were performed by Nishino et al. (2007) for a circular cylinder near a moving wall for higher Reynolds numbers ($O(10^5)$). For a cylinder with endplates, they reported that the flow essentially remained two-dimensional, with Bénard–von Kármán type vortices being shed for gap heights $G/D > 0.5$, and an intermediate shedding regime was observed in the range $0.35 \leq G/D \leq 0.5$. Complete cessation of shedding occurred for $G/D < 0.35$. However, for a cylinder without endplates, they reported that Bénard–von Kármán type wake vortices were not being generated, and a near constant drag coefficient was recorded.

Huang and Sung (2007) performed two-dimensional simulations for a circular cylinder moving near a wall for gap heights in the range $G/D > 0.1$ for $Re \leq 600$. The gap heights at which alternate vortex shedding disappeared decreased from $0.28D$ to $0.25D$ as the Reynolds number was increased from 300 to 600. The non-dimensionalised shedding frequency ($St = fD/U$, with f the shedding frequency) at different Reynolds numbers increased as the cylinder was brought close to the wall ($\approx 0.5D$), followed by a rapid decrease as the gap height was decreased. They further quantified the lift and drag coefficients, with the lift coefficient showing a linear increase as the cylinder was brought closer to the wall. They however acknowledged their restriction of two-

dimensional simulations, and hence did not rule out possible important three-dimensional effects over their parameter range.

In a similar study by Yoon et al. (2010), numerical investigations were performed for a circular cylinder moving parallel to a wall for $Re \leq 200$ at different gap heights using an immersed boundary technique. The time-averaged lift and drag coefficients decreased exponentially as the gap height was increased to higher values. The onset of vortex shedding was delayed to higher Reynolds numbers as the gap height was decreased. Vortex shedding persisted at $Re = 120$ for the cylinder moving at a gap height of $G/D = 0.1$.

Arnal et al. (1991) investigated the flow structures for a square cylinder sliding along a wall. Their numerical simulations showed that periodic flow was observed for $Re > 100$, with vortex pairs convecting downstream after formation, and moving further away from the sliding wall. However, for the case of a fixed wall, vortex pairs formed but convected parallel to the lower wall.

The ground effect of a half-cylinder using a moving ground for Reynolds numbers between $6.8 \times 10^4 \leq Re \leq 1.7 \times 10^5$ was investigated by Zhang et al. (2005). The critical gap height at which vortex shedding was suppressed was in the range $0.525 \leq G/D \leq 0.55$. The drag force was nearly constant below this height and a sharp increase to twice the value was observed around the critical gap height. The lift coefficient decreased as the gap height was increased. Furthermore, the Strouhal number was invariant to the gap height.

Zerihan and Zhang (2000) investigated the variation of force coefficients on a single element wing (of chord c) at high Reynolds numbers ($O(10^4)$). For their airfoil tested, the (negative) lift coefficient increased from low gap heights to a maximum value at height $h/c = 0.08$, beyond which a decrease in the lift coefficient was observed. The drag coefficient decreased with increasing gap height. They further varied the incidence angle of the airfoil and observed that the gap height at which the maximum (negative) lift was generated varied marginally, reducing the sensitivity to ride height.

Rao et al. (in press) investigated the variation in flow structures for a circular cylinder translating parallel to a wall at different gap heights for $Re \leq 200$. As the gap height was reduced from $G/D = \infty$ (free-stream) to $G/D \to 0$, the onset of unsteady flow was delayed to higher Reynolds numbers. For $G/D \geq 0.3$, alternate vortex shedding was observed in the flow, accompanied by an increase in the shedding frequency. They further investigated the onset of three-dimensionality at various gap heights. For $G/D \geq 0.28$, the onset of three-dimensional flow occurred in the unsteady regime, while for gap heights below this value, three-dimensionality occurred in the steady regime. For bodies near a wall, they observed that several modes became unstable in the unsteady regime. Their three-dimensional direct numerical simulations (DNS) showed that the flow eventually becomes chaotic, possibly due to non-linear interactions of these modes.

In further investigations of cylinders near a wall, Stewart et al. (2006, 2010) and Rao et al. (2011) investigated the effect of rotation for translating cylinders near a wall for $Re \leq 750$. Relative to the non-rotating case, for forward rolling cylinders, the transition to periodic wake flow occurred at lower Reynolds numbers, while for reverse rolling, the transition was delayed to higher Reynolds numbers, with vortex shedding ceasing altogether for $\alpha \leq -1.5$. Three-dimensional flow occurred at lower Reynolds numbers for forward rolling cylinders, while for reverse rolling cylinder, the transition was delayed to higher Reynolds numbers. For $\alpha = -2$, the flow remained two-dimensional for $Re \leq 750$. Their experimental investigations in a water tunnel confirmed the flow structures predictednumerically.

The flows past a circular cylinder moving near a free-slip surface at different gap heights for different Froude numbers were investigated by Reichl et al. (2005). For the zero-Froude-number case corresponding to a non-deformable surface, vortex shedding was observed for gaps greater than $0.15D$. At smaller gap heights, vortex shedding was suppressed, while for gap heights greater than $0.5D$, vortex shedding appeared similar to regular Bénard–von Kármán shedding. For non-zero Froude numbers, surface deformation was observed downstream of the cylinder at low gap heights, and for larger gap heights a surface jet was observed. The shedding frequency increased as the gap height was increased from low values to $G/D \approx 0.8$, followed by a decrease as the submergence depth was further increased.

The aims of this paper are

- to review briefly how vorticity is generated at boundaries, redistributed into the flow, and interacts with other boundaries;
- to examine the 3D transitions that arise in the vorticity generated at, and shed from, circular cylinders;
- to evaluate the effect of wall proximity and cylinder rotation on wake structures and transitions.

The structure of this article is as follows. After the description of the flow problem and methods, we first review the important previous works of Morton (1984) and Lundgren and Koumoutsakos (1999) to understand the generation and conservation of vorticity at both solid and stress-free surfaces. Following this, the two-dimensional modes of shedding from a circular cylinder are reviewed for an isolated cylinder, a cylinder moving parallel to a wall for decreasing gap widths, and then the addition of both pro- and retro-grade rotation of the cylinder are considered. Next, the development of three-dimensional wakes modes from the initial two-dimensional vorticity shed from cylinders is studied, with emphasis on the difference in the order of appearance and characteristics of the modes. Finally, a discussion of the effect of wall proximity and cylinder rotation on the wake structures and stability is presented, followed by concluding remarks.

2. Problem definition and methodology

The schematic representation of the cylinder moving parallel to the wall is shown in Fig. 1. The cylinder of diameter D is moving at a gap height of G from the wall. However, in the numerical setup, the frame of reference is centred at the cylinder, with the fluid and the lower wall moving at an uniform speed and the cylinder stationary. The controlling parameter is the Reynolds number, $Re = UD/\nu$, where ν is the kinematic viscosity of the fluid. It is varied here over the range $25 \leq Re \leq 750$. The computational domains were constructed for different gap heights from freestream ($G/D = \infty$) to

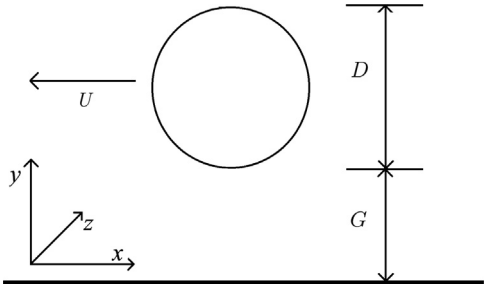

Fig. 1. Schematic representation of the circular cylinder of diameter D at a distance G from a stationary wall. The cylinder translates at a constant speed U to the left. For the numerical simulations, the frame of reference is attached to the cylinder. In that frame the cylinder is stationary, while the fluid and wall move at a constant speed U to the right.

near wall ($G/D=0.005$). The small gap was maintained to prevent singular mesh elements between the bottom of the cylinder and the lower wall. Previous studies (Rao et al., 2011; Stewart et al., 2006, 2010) have shown good agreement between the flow structures visualised in the experiments and those observed numerically, although the force coefficients recorded are more sensitive to this gap height. For this numerical study, the cylinder was modelled as a smooth body.

As the body moves through the non-Newtonian fluid, both viscous and pressure forces act on it. The lift force (F_l) and drag force (F_d) are normalised by the dynamic pressure and frontal area per unit width ($0.5\rho U^2 D$) to obtain the lift and drag coefficients, respectively. In the unsteady regime of flow, vortex shedding occurs and the force coefficients vary periodically. In those cases, time-averaged quantities are reported. The frequency of shedding f is normalised by the cylinder diameter and flow speed, thereby obtaining the Strouhal number, given by $St=fD/U$.

2.1. Numerical formulation

The incompressible Navier–Stokes equations are solved using a spectral-element method based on the Galerkin finite-element method. The computational domain is constructed from quadrilateral elements, mainly rectangular, while some have curved boundaries to model the surface of the cylinder. These macro-elements are further subdivided into internal node points, which are distributed according to the Gauss–Legendre–Lobatto quadrature points, with the velocity and pressure fields represented by a tensor product of Lagrangian polynomial interpolants within the elements. Such methods are known to provide spectral convergence as the number of internal nodes per element (N) is increased (Karniadakis and Sherwin, 2005). The number of node points is specified at runtime, with the interpolant polynomial order being $N-1$. A fractional time-stepping technique is used to integrate the advection, pressure and diffusion terms of the Navier–Stokes equation (Karniadakis et al., 1991; Chorin, 1968). The unsteady solver is used to investigate the parameter range covering both the steady and unsteady regimes of flow. More details on this method can be found in Thompson et al. (2006a). It has been used previously in related studies of bluff bodies in a free-stream (Thompson et al., 1996; Leontini et al., 2007; Thompson et al., 2006b), and for bodies near a wall (Stewart et al., 2006, 2010; Rao et al., 2011), and for spheres and cylinders impacting a wall (Leweke et al., 2004; Thompson et al., 2007).

2.2. Linear stability analysis

The onset of three-dimensionality is an important aspect in the understanding of bluff body flows as a route to chaos and fully turbulent flow. For an isolated cylinder, three-dimensional flow first occurs at $Re\approx188$ (Barkley and Henderson, 1996) after the wake has already undergone a transition to two-dimensional periodic flow at $Re\approx47$. For bodies close to a wall, the transition sequence is reversed, with the flow becoming three dimensional prior to becoming unsteady (Stewart et al., 2010; Rao et al., 2011). We here investigate the variation between these two extremities, mapping the variation at different gap heights. Linear stability analysis is used to determine the growth or decay of infinitesimal spanwise sinusoidal perturbations imposed on the two-dimensional steady or unsteady base flow. Numerically, the Navier–Stokes equations are linearised and the spanwise perturbation fields can be expressed as a sum over Fourier modes corresponding to different spanwise wavelengths (λ). Linearity of the equations allows examination of each Fourier mode separately. The resulting equations are marched forward in time, and after several periods, the fastest growing modes dominate the system. For unsteady flows, the period of monitoring the solution is equal to the period of the base flow period (T), while an arbitrary time period is chosen for cases with a steady base flow. The ratio of the magnitude of the perturbation field over consecutive periods is denoted by $\mu=e^{\sigma T}$, where μ is the Floquet multiplier (for periodic base flows) or the amplification factor, and σ is the growth rate. For exponentially growing modes, the Floquet multiplier returns a value of $\mu>1$, or a positive growth rate ($\sigma>0$). A parameter space over a range of Reynolds number and normalised spanwise wavelengths (λ/D) is mapped, obtaining the value of the Floquet multiplier/growth rate. Polynomial interpolation is then carried out to obtain the critical values at which the flow becomes unstable to three-dimensional perturbations.

For a circular cylinder wake, the first two fastest-growing three-dimensional modes are purely real, with the periodicity of the three-dimensional perturbations being commensurate with the base flow period. However, other modes that are incommensurate with the base flow have been found in the wakes of circular and square cylinders, where the Floquet multiplier has a complex component (Robichaux et al., 1999; Blackburn and Lopez, 2003). Modes whose periods are twice the period of the base flow have been found in the wake behind rings and are termed sub-harmonic modes (Sheard et al., 2005a, 2005b).

2.3. Resolution studies

The computational domain used for the two-dimensional flow computations had boundaries at significantly large distances from the cylinder-wall system. The inlet and outlet boundaries where placed at $100D$ from the cylinder, while the upper boundary was located $150D$ from the lower wall. The computational domain and mesh system used is similar to that shown in Fig. 2 of Stewart et al. (2010). The macroelements were concentrated in the vicinity of the cylinder and were distributed sparsely $30D$ away from the cylinder. Similar studies conducted by Rao et al. (2011) showed minimal variations of the force coefficients and Strouhal number for the maximum tested flow speed. Furthermore, spatial resolution studies were conducted for $G/D=0.01$ at $Re=200$ by varying the polynomial order of the interpolants between $N^2=4^2$ and 10^2. For $N^2=7^2$, maximum variation in the force coefficients and Strouhal number was less than 0.1%. However, to ensure adequate resolution of the flow structures in the far wake and to capture the spanwise component of flow, the resolution of the macroelements was increased to $N^2=9^2$. Further, to ensure stability of the solver at these resolutions, the time-step used was $0.001D/U$.

3. Results

3.1. Two-dimensional flows

3.1.1. Review of vorticity generation and conservation

A dynamical formulation for the generation of vorticity has previously been presented by Morton (1984) for an incompressible, homogeneous, Newtonian fluid. Considering mainly the flow next to a solid wall, it was concluded that

1. Vorticity is generated instantaneously at boundaries by the relative acceleration of the fluid and wall produced:
   (a) from the fluid side by tangential pressure gradients;
   (b) from the wall side by acceleration of the boundary, where generation is again partially masked by viscous diffusion when there is continuing generation.
2. For an impulsive change, wall stress does not produce vorticity.
3. The only means of decay or loss of vorticity is by cross-diffusion and annihilation of vorticity of opposite signs.

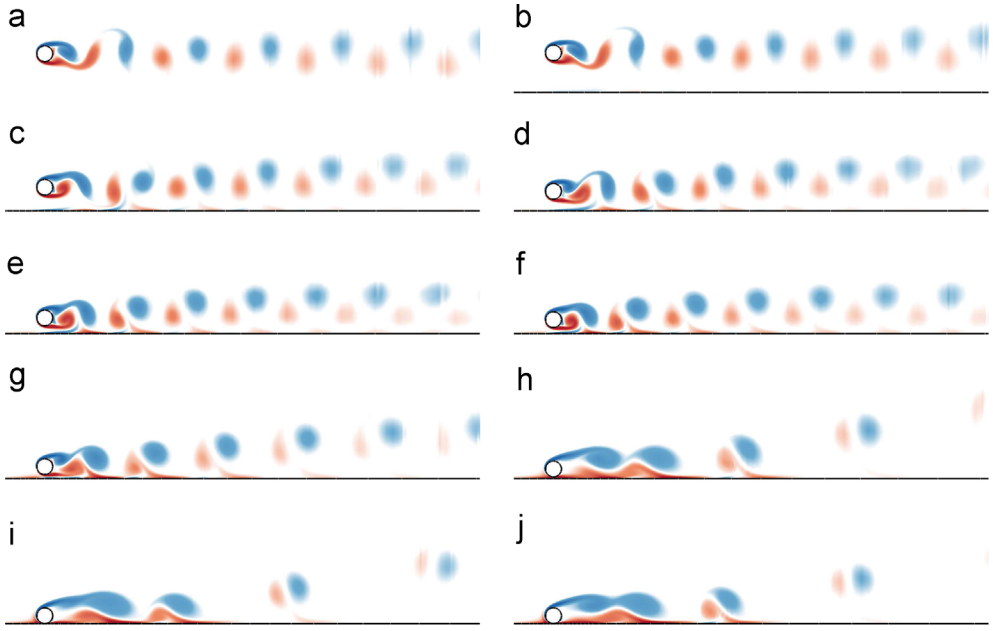

Fig. 2. Flow structures at $Re=180$ for the circular cylinder moving from right to left at the specified gap heights. Vorticity contours levels are between $\pm 5D/U$. The wake is visualised for a streamwise distance in excess of $25D$ downstream of the cylinder. (a) $G/D\rightarrow\infty$. (b) $G/D=2$. (c) $G/D=1$. (d) $G/D=0.75$. (e) $G/D=0.5$. (f) $G/D=0.4$. (g) $G/D=0.25$. (h) $G/D=0.1$. (i) $G/D=0.01$. (j) $G/D=0.005$. Red and blue shading is used to indicate positive and negative vorticity contours, respectively. (For interpretation of the references to color in this figure caption, the reader is referred to the web version of this article.)

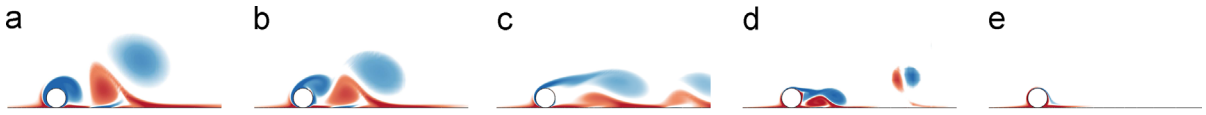

Fig. 3. Flow structures at the specified rotation rates and Reynolds numbers captured at the instant of maximum instantaneous lift coefficient. The contour levels are between $\pm 5D/U$. (a) $\alpha=+2$, $Re=180$. (b) $\alpha=+1$, $Re=180$. (c) $\alpha=0, Re=180$. (d) $\alpha=-1, Re=750$. (e) $\alpha=-2, Re=750$.

The case of a stress-free surface has also been studied, and it has been shown that vorticity is conserved (Lundgren and Koumoutsakos, 1999). That is, vorticity (in terms of total circulation) is not lost through the free surface but rather is "stored" in the vortex sheet representing the free surface. This is an important result that needs to be considered in our analyses.

The findings of Morton (1984) and Lundgren and Koumoutsakos (1999) provide guidelines for our understanding of the origin and conservation of vorticity in cylinder wakes in the following cases.

3.1.2. *Non-rotating translating cylinder and wall effect*

Shown in Fig. 2 are the vortical wake flow structures for a circular cylinder translating parallel to a solid wall at $Re=180$, for various gap heights. The red and blue shading indicates negative and positive vorticity, respectively, originating from the detached shear layers from the translating cylinder. Because the integrated tangential pressure gradient around the whole cylinder must necessarily be zero, then according to Morton (1984), the net vorticity generation is also zero. That is, equal amounts of positive and negative vorticity are generated. For an isolated cylinder, vortex shedding occurs alternately from the upper and lower separation points, and the shed vortices form what is commonly known as a "Bénard–von Kármán vortex street". As the gap height is decreased to ≈0.25, single-sided vortex shedding occurs, where the shear layers separating from the top of the cylinder combines with the wall shear layer vorticity to form a vortex pair, which advects away from the wall as it moves downstream. Clearly discernible from these images is the drop in shedding frequency as the cylinder is positioned closer to the wall.

The critical Reynolds number for the transition to unsteady flow increases from $Re_c\approx47$ for $G/D\rightarrow\infty$ to $Re_c\approx160$ as $G/D\rightarrow0$. This clearly indicates the stabilising effect of the wall, delaying the onset of periodic flow. The Strouhal number or non-dimensional shedding frequency, $St=fD/U$, with f the frequency, is a function of both the Reynolds number and the gap height. This variation has been documented in Fig. 6 of Rao et al. (in press) for $Re\leq200$.

3.1.3. *Rotating cylinder translating on a wall*

We now consider the case of the circular cylinder rolling along a wall at different rotation rates ($-2\leq\alpha\leq2$). Again, equal amounts of opposite-signed vorticity are generated over the cylinder surface. Pressure gradients are also induced on the wall and therefore vorticity is generated there locally. As the rotation rate is increased to higher positive values, the onset of vortex shedding is observed at lower Reynolds numbers, while on decreasing the rotation rate to negative values, the onset of shedding is delayed to higher Reynolds numbers. It is suppressed entirely for $\alpha\leq-1.5$ for $Re\leq750$ (also see Fig. 7). Fig. 3 shows the flow structures observed in the wake of the rotating cylinder. The process of vortex shedding for these cases has been shown in Fig. 13 of Stewart et al. (2010) and in Fig. 4 of Rao et al. (2011). Furthermore, comparison of these flow structures with experimental dye visualisations has been shown in Figs. 15 and 16 of Stewart et al. (2010) and in Fig. 12 of Rao et al. (2011).

3.1.4. *Cylinder rolling in reverse along a free slip surface*

Shown in Fig. 4 is the comparison between the flow structures for a cylinder rolling in reverse along a no-slip wall with those for a slip wall. The process of shedding in the two cases is vastly

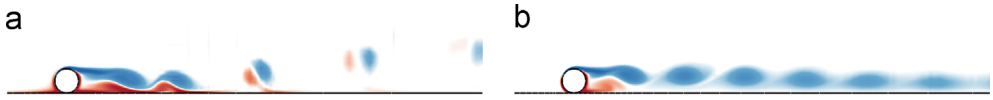

Fig. 4. Flow structures for a reverse rolling cylinder at $\alpha=-1$, $Re=450$ along (a) a no-slip surface and (b) a slip surface. The contour levels for both images are between $\pm 5D/U$. The Strouhal numbers for the no-slip and slip cases are 0.218 and 0.196, respectively.

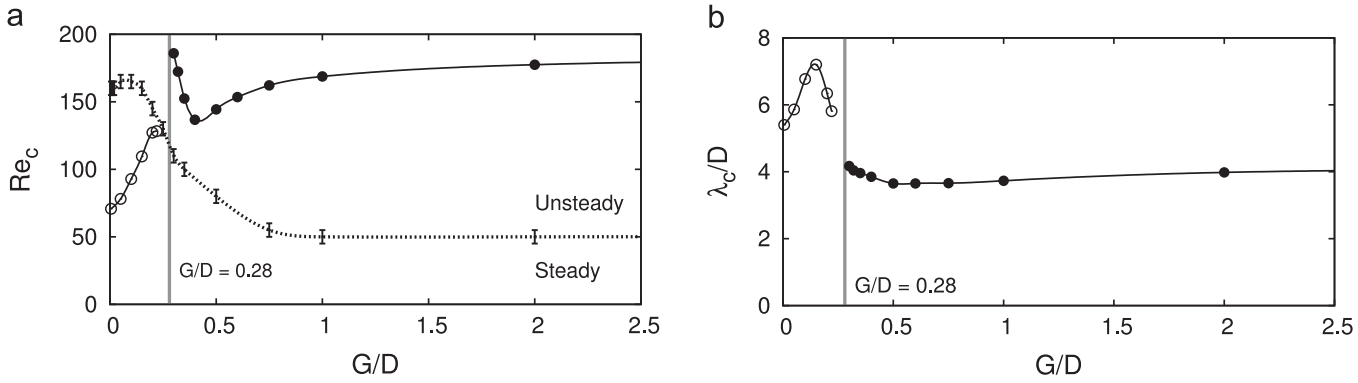

Fig. 5. (a) Transition diagram showing the variation of the critical Reynolds number for the onset of three-dimensional flow and as gap height is increased from $G/D\approx 0$ to $G/D=2.5$. The steady–unsteady transition is represented by the dotted line over this range. The open circles (○) indicate the critical Reynolds number for the onset of three-dimensional transition for $G/D\leq 0.25$ in the steady regime of flow and closed circles (●) indicate the critical Reynolds number for the onset of three-dimensional transition for $G/D\geq 0.25$ in the unsteady regime. (b) Variation of the critical spanwise wavelength with gap height. Figures from Rao et al. (in press).

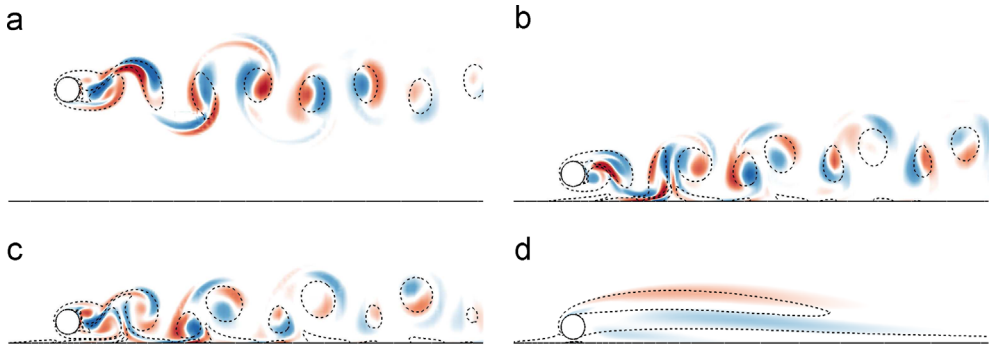

Fig. 6. Spanwise perturbation vorticity contours for the cylinder translating parallel to a wall at the specified gap height and Reynolds number. For $G/D\leq 0.25$, the transition to three-dimensionality occurs in the steady regime of flow, while for $G/D>0.25$, the transition occurs in the unsteady regime. The contour shading is between levels $\pm 0.1D/U$, and the dashed lines show the base flow vorticity contour levels between $\pm 1D/U$. (a) $G/D=4$, $Re=180$, $\lambda/D=4$. (b) $G/D=0.6$, $Re=165$, $\lambda/D=3.6$. (c) $G/D=0.35$, $Re=165$, $\lambda/D=4$. (d) $G/D=0.15$, $Re=120$, $\lambda/D=8$.

different. For the no-slip wall, vorticity from the top shear layer combines with opposite-signed vorticity generated beneath it at the wall to form a vortex pair which moves parallel to the wall. In the case of a slip wall, a single-sided vortex is shed, which then translates along the surface. In terms of vorticity generation, the pressure gradient along the interface at the free-slip surface generates vorticity (in the form of a vortex sheet, as presented by Lundgren and Koumoutsakos (1999). The total vorticity in the system is found to be conserved. However, as opposed to the no-slip wall, vorticity cannot diffuse out of the planar free-slip surface, and therefore we do not see the vortices of the opposite sign being formed at the wall in this case.

3.2. Transition to three-dimensionality

For an isolated cylinder translating in a free stream, the onset of three-dimensional flow occurs for an unsteady base flow at $Re_c\approx 190$ (Barkley and Henderson, 1996), while for a non-rotating cylinder almost touching a no-slip wall, the transition occurs in the steady regime at $Re\approx 71$ (Stewart et al., 2010). For the intermediate gap heights, this transition is mapped and is shown in Fig. 5. Fig. 5(a) shows the variation of the critical Reynolds number for the transition to three-dimensional flow as the gap height is varied. For $G/D\leq 0.25$, the transition occurs in the steady regime and shows a monotonic rise in critical Reynolds number as the gap height is increased. For $G/D\geq 0.25$, the transition occurs on an unsteady base flow. At $G/D=0.28$, the flow was found to remain two-dimensional for $Re\leq 200$. At greater gap heights of $G/D\geq 0.6$, the critical Reynolds number approaches that observed for an isolated cylinder (Rao et al., in press). Fig. 5(b) shows the variation of the critical spanwise wavelength at the onset of three-dimensional flow. At large gap heights, the onset of three-dimensionality manifests as the mode A instability, with a critical spanwise wavelength of $\approx 4D$.

Fig. 6 shows the spanwise perturbation vorticity contours at Reynolds numbers slightly greater than the critical values for the onset to three-dimensional flow. At large gap heights, the contours resemble the mode A type instability observed for bodies in isolation. Although the gap height is decreased to $\approx 0.3D$, the signature of the mode A is retained, with vortex shedding predominantly becoming single sided. At very low gap heights ($G/D\leq 0.2$), the transition to three-dimensionality occurs in the steady flow with the spanwise perturbations growing in the recirculation regions.

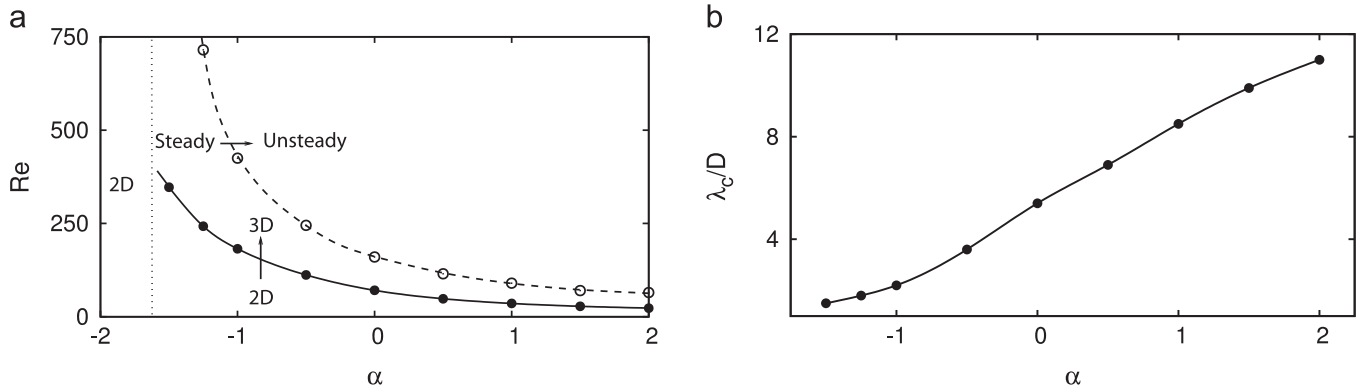

Fig. 7. (a) Variation of the critical Reynolds numbers for the onset of unsteady flow (○) and three-dimensional flow (•) for cylinders sliding and rotating along a wall. (b) Variation of the critical spanwise wavelength with rotation rate.

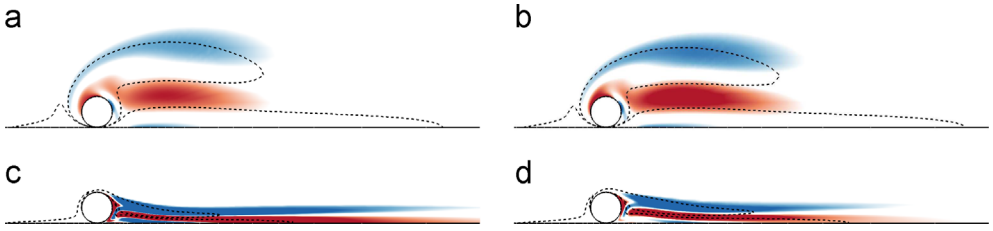

Fig. 8. Spanwise perturbation vorticity contours for the cylinder rolling along a wall at the specified rotation rate. The contour shading is between levels $\pm 0.1D/U$, and the dashed lines show the base flow vorticity contour levels between $\pm 1D/U$. (a) $\alpha = +2$, $Re = 25$, $\lambda/D = 11$. (b) $\alpha = +1.5$, $Re = 30$, $\lambda/D = 10$. (c) $\alpha = -1.25$, $Re = 250$, $\lambda/D = 1.8$. (d) $\alpha = -1.5$, $Re = 400$, $\lambda/D = 1.5$.

For cylinders on a wall, the onset of three-dimensional flow occurs at lower Reynolds number as the positive rotation rate is increased, while for negative rotation rates, the onset occurs at higher Reynolds number. For rotation rates $\alpha < 1.5$, the flow remains two-dimensional for $Re \leq 750$. Fig. 7(a) shows this variation on an α–Re plot. This figure also shows the critical Reynolds number for the onset of unsteady flow as the rotation rate is varied. As the rotation rate is increased from negative values, the onset of three-dimensionality occurs at lower Reynolds number. A similar trend is observed with respect to onset of unsteady flow. Fig. 7(b) shows the variation of the critical spanwise wavelength with rotation rate. As the rotation rate is increased, the spanwise wavelength at which the flow becomes three-dimensional monotonically increases.

Spanwise perturbation vorticity contours obtained from stability analysis are shown in Fig. 8 for selected rotation rates. These coloured contour plots show regions in the wake of the rolling cylinder where the fastest-growing three-dimensional mode has the large amplitudes. The variation in the spanwise direction is sinusoidal. Not surprisingly, the amplification of the instability is associated with the attached regions of positive and negative spanwise vorticity in the wake. For other rotation rates, the reader is referred to Figs. 22 and 23 of Stewart et al. (2010).

For cylinders near a wall, multiple unstable three-dimensional modes can be identified after the wake has already undergone a transition to unsteady periodic flow. Rao et al. (in press) observed four modes for a cylinder sliding along a wall at $Re = 200$. Furthermore, they performed three-dimensional Direct Numerical Simulations (DNS) to investigate the nonlinear interactions between these (linear) modes. While the wake was observed to be periodic initially, the flow evolved to be chaotic, no longer resembling the two-dimensional periodic base flow.

The effect of a nearby wall on a cylinder wake is therefore profound. For a translating cylinder located close to a wall ($G/D < 0.25$), direct shedding of vortices from the lower side of the cylinder ceases. The transition to three-dimensionality in this case occurs prior to the transition to an unsteady wake. In the case of a no-slip wall, secondary vorticity is generated at a wall via a tangential pressure gradient induced by a primary vortex above it. That secondary vorticity initially diffuses away from the wall before being advected by the flow to form a vortex structure. The opposite-signed primary and secondary vortices pair and self-propel away from the wall. In the case of a free-slip surface, some secondary vorticity is induced at the back surface of the cylinder, which diffuses out slowly but it does not form identifiable vortex structures. Vorticity is also generated at the free-slip surface but it is trapped there and cannot diffuse away. In this case, apart from some opposite-signed vorticity close the cylinder, the wake consists of vortices of a single sign. The effect of rotation of a cylinder translating along the wall is to accentuate the shedding and pairing in the case of increasing prograde rotation, and to mitigate this effect in the case of increasing retrograde rotation, with vortex shedding eventually becoming suppressed as the retrograde rotation rate is increased.

4. Conclusions

Vorticity generation at a boundary has been reviewed, with the identified mechanisms being a tangential acceleration of the boundary or a tangential pressure gradient in the fluid at the boundary. Subsequent redistribution of the vorticity occurs through diffusion away from the boundary and then advection with the fluid. Vorticity (in terms of total circulation) is conserved and cannot be lost at a boundary; for the special case of a slip boundary, vorticity is stored at the boundary interface in the form of a vortex sheet.

We have investigated the flow past a circular cylinder translating parallel to, and at different distances from, a wall using spectral-element simulations. Two-dimensional simulations showed the onset of unsteady flow in the wake was delayed to higher Reynolds numbers as the gap height was decreased, except very

close to the wall ($G/D \leq 0.1$). Using linear stability analysis, we studied the variation of the critical Reynolds number and the associated spanwise wavelength for different gap heights for three-dimensional transition. For $G/D \leq 0.25$, the transition occurs while the wake is still steady. Beyond this gap height, three-dimensional flow transition is delayed until after the wake has already become unsteady. The critical Reynolds numbers for $G/D = 0.3$ and 0.4 are $Re_c = 185$ and 137, respectively. Above $G/D = 0.4$ the critical Reynolds number increases monotonically towards the value observed for an isolated cylinder ($Re \approx 188$) (Barkley and Henderson, 1996).

The effect of cylinder rotation on wake transitions has also been quantified. In general, forward (or prograde) rolling reduces the critical Reynolds number, while reverse (or retrograde) rolling has the opposite effect. When the cylinder is close to a wall, strong retrograde rolling encourages the wake to wrap around the cylinder, thereby reducing the height of the wake and the cross-stream size of positive and negative vorticity regions within it. For $\alpha = -2$, three-dimensional transition was suppressed up to $Re = 750$.

Clearly, the presence of a wall and cylinder rotation strongly affect wake development both qualitatively and quantitatively. This is especially apparent in terms of vorticity injected into the flow, trapped vorticity at free-slip surfaces, subsequent wake dynamics, and the initial transition to either three-dimensional steady or two-dimensional unsteady wake flow. Furthermore, wall proximity and rotation affect the appearance and stability of three-dimensional wake modes, which in turn strongly affect the path to wake turbulence at higher Reynolds numbers.

Acknowledgments

The support from Australian Research Council Discovery Grants DP110100434 and DP130100822 and computing time from the National Computational Infrastructure (NCI), the Victorian Life Sciences Computation Initiative (VLSCI) and the Monash Sungrid are gratefully acknowledged.

References

Akoury, R.E., Braza, M., Perrin, R., Harran, G., Hoarau, Y., 2008. The three-dimensional transition in the flow around a rotating cylinder. Journal of Fluid Mechanics 607, 1–11.
Arnal, M., Goering, D., Humphrey, J.A.C., 1991. Vortex shedding from a bluff body adjacent to a plane sliding wall. ASME Journal of Fluids Engineering 113, 384–398.
Bailey, S., Martinuzzi, R., Kopp, G., 2002. The effects of wall proximity on vortex shedding from a square cylinder: three-dimensional effects. Physics of Fluids 14, 4160–4177.
Barkley, D., Henderson, R.D., 1996. Three-dimensional Floquet stability analysis of the wake of a circular cylinder. Journal of Fluid Mechanics 322, 215–241.
Batchelor, G.K., 1967. An Introduction to Fluid Dynamics. Cambridge University Press, Cambridge, UK.
Bearman, P.W., Zdravkovich, M.M., 1978. Flow around a circular cylinder near a plane boundary. Journal of Fluid Mechanics 89, 33–47.
Blackburn, H.M., Lopez, J.M., 2003. On three-dimensional quasiperiodic Floquet instabilities of two-dimensional bluff body wakes. Physics of Fluids 15, L57–L60.
Cheng, M., Luo, L.S., 2007. Characteristics of two-dimensional flow around a rotating circular cylinder near a plane wall. Physics of Fluids 19.
Chorin, A.J., 1968. Numerical solution of the Navier–Stokes equations. Mathematics of Computation 22, 745–762.
Huang, W.X., Sung, H.J., 2007. Vortex shedding from a circular cylinder near a moving wall. Journal of Fluids and Structures 23, 1064–1076.
Kang, S.M., Choi, H.C., Lee, S., 1999. Laminar flow past a rotating circular cylinder. Physics of Fluids 11.
Karniadakis, G.E., Israeli, M., Orszag, S.A., 1991. High-order splitting methods of the incompressible Navier-Stokes equations. Journal of Computational Physics 97, 414–443.
Karniadakis, G.E., Sherwin, S.J., 2005. Spectral/HP Methods for Computational Fluid Dynamics. Oxford University Press, Oxford.
Karniadakis, G.E., Trintafyllou, G.S., 1992. Three-dimensional dynamics and transition to turbulence in the wake of bluff objects. Journal of Fluid Mechanics 238, 1–30.
Kumar, S., Cantu, C., Gonzalez, B., 2011. Flow past a rotating cylinder at low and high rotation rates. Journal of Fluids Engineering 133, 041201.
Lei, C., Cheng, L., Armfield, S., Kavanagh, K., 2000. Vortex shedding suppression for flow over a circular cylinder near a plane boundary. Ocean Engineering 27, 1109–1127.
Leontini, J., Thompson, M.C., Hourigan, K., 2007. Three-dimensional transition in the wake of transversely oscillating cylinder. Journal of Fluid Mechanics 577, 79–104.
Leweke, T., Thompson, M.C., Hourigan, K., 2004. Vortex dynamics associated with the collision of a sphere with a wall. Physics of Fluids (Letters) 16, L74–L77.
Lundgren, T., Koumoutsakos, P., 1999. On the generation of vorticity at a free surface. Journal of Fluid Mechanics 382, 351–366.
Mahir, N., 2009. Three-dimensional flow around a square cylinder near a wall. Ocean Engineering 36, 357–367.
Mittal, S., Kumar, B., 2003. Flow past a rotating cylinder. Journal of Fluid Mechanics 476, 303–334.
Morton, B.R., 1984. The generation and decay of vorticity. Geophysical and Astrophysical Fluid Dynamics 28, 277–308.
Nishino, T., Roberts, G.T., Zhang, 2007. Vortex shedding from a circular cylinder near a moving ground. Physics of Fluids 19, 025103.
Pralits, J.O., Brandt, L., Giannetti, F., 2010. Instability and sensitivity of the flow around a rotating circular cylinder. Journal of Fluid Mechanics 650, 513–536.
Price, S.J., Sumner, D., Smith, J., Leong, K., Paidoussis, M., 2002. Flow visualization around a circular cylinder near to a plane wall. Journal of Fluids and Structures 16, 175–191.
Rao, A., Leontini, J., Thompson, M.C., Hourigan, K., 2013. Three-dimensionality in the wake of a rotating cylinder in a uniform flow. Journal of Fluid Mechanics 717, 1–29.
Rao, A., Stewart, B.E., Thompson, M.C., Leweke, T., Hourigan, K., 2011. Flows past rotating cylinders next to a wall. Journal of Fluids and Structures 27, 668–679.
Rao, A., Thompson, M.C., Leweke, T., Hourigan, K., The flow past a circular cylinder translating at different heights above a wall. Journal of Fluids and Structures, http://dx.doi.org/10.1016/j.jfluidstructs.2012.08.007, in press.
Reichl, P., Hourigan, K., Thompson, M., 2005. Flow past a cylinder close to a free surface. Journal of Fluid Mechanics 533, 269–296.
Robichaux, J., Balachandar, S., Vanka, S.P., 1999. Three-dimensional Floquet instability of the wake of square cylinder. Physics of Fluids 11, 560–578.
Roshko, A., 1954. On the drag and shedding frequency of two-dimensional bluff bodies. Technical Report. NACA Technical Report Number 3169.
Sheard, G., Thompson, M., Hourigan, K., 2005a. The evolution of a subharmonic mode in a vortex street. Journal of Fluid Mechanics 534, 23–38.
Sheard, G., Thompson, M., Hourigan, K., 2005b. The subharmonic mechanism of the mode C instability. Physics of Fluids 17, 111702.
Stewart, B.E., Hourigan, K., Thompson, M.C., Leweke, T., 2006. Flow dynamics and forces associated with a cylinder rolling along a wall. Physics of Fluids 18, 111701-1–111701-4.
Stewart, B.E., Thompson, M.C., Leweke, T., Hourigan, K., 2010. The wake behind a cylinder rolling on a wall at varying rotation rates. Journal of Fluid Mechanics 648, 225–256.
Stojković, D., Schön, P., Breuer, M., Durst, F., 2003. On the new vortex shedding mode past a rotating circular cylinder. Physics of Fluids 15, 1257–1260.
Taneda, S., 1965. Experimental investigation of vortex streets. Journal of the Physical Society of Japan 20, 1714–1721.
Thompson, M., Leweke, T., Hourigan, K., 2007. Sphere-wall collision: vortex dynamics and stability. Journal of Fluid Mechanics 575, 121–148.
Thompson, M.C., Hourigan, K., Cheung, A., Leweke, T., 2006a. Hydrodynamics of a particle impact on a wall. Applied Mathematical Modelling 30, 1356–1369.
Thompson, M.C., Hourigan, K., Ryan, K., J., G., 2006b. Wake transition of two-dimensional cylinders and axisymmetric bluff bodies. Journal of Fluids and Structures 22, 793–806.
Thompson, M.C., Hourigan, K., Sheridan, J., 1996. Three-dimensional instabilities in the wake of a circular cylinder. Experimental Thermal and Fluid Science 12, 190–196.
Williamson, C.H.K., 1988. The existence of two stages in the transition to three dimensionality of a cylinder wake. Physics of Fluids 31, 3165–3168.
Williamson, C.H.K., 1996. Vortex dynamics in the cylinder wake. Annual Review of Fluid Mechanics 28, 477–539.
Wu, J., Sheridan, J., Welsh, M.C., Hourigan, K., 1996. Three-dimensional vortex structures in a cylinder wake. Journal of Fluid Mechanics 312, 201–222.
Yoon, H., Lee, J., Seo, J., Park, H., 2010. Characteristics for flow and heat transfer around a circular cylinder near a moving wall in wide range of low Reynolds number. International Journal of Heat and Mass Transfer 53, 5111–5120.
Zerihan, J., Zhang, X., 2000. Aerodynamics of a single element wing in ground effect. Journal of Aircraft 37, 1058–1064.
Zhang, X., Mahon, S., Den-Berg, M.V., Williams, C., 2005. Aerodynamics of a half-cylinder in ground effect. In: Engineering Turbulence Modelling and Experiments, vol. 6. Elsevier Science B.V., pp. 461–470.